Advances in Science and Technology Research Journal

Advances in Science and Technology Research Journal, 2026, 20(8), 333–359
https://doi.org/10.12913/22998624/221647
ISSN 2299-8624, License CC-BY 4.0

Received: 2026.04.02
Accepted: 2026.04.07
Published: 2026.07.01

Vibration-based fatigue life prediction of glass fibre reinforced polymer laminates using modal frequency degradation with semi-empirical and machine learning models

Rahul Bakthavathchalam[1,2], Avinash Lakshmikanthan[3,4*], C.M. Vigneswaran[5], S.P. Prashanth[6]

[1] Department of Aeronautical Engineering, Nitte Meenakshi Institute of Technology, Nitte (Deemed to be University), Bengaluru, Karnataka, India
[2] Visvesvaraya Technological University, Belagavi, Karnataka 590018, India
[3] Department of Mechanical Engineering, Nitte Meenakshi Institute of Technology, Nitte (Deemed to be University), Bengaluru, Karnataka, India
[4] Research Fellow, INTI International University, Persiaran Perdana BBN, Putra Nilai, Nilai 71800, Negeri Sembilan, Malaysia
[5] Department of Aerospace Engineering, Ramaiah Institute of Technology, Bengaluru, Karnataka, India
[6] Department of Mechanical Engineering, Presidency School of Engineering, Presidency University, Bengaluru, Karnataka, India
* Corresponding author's e-mail: avinash.l@nmit.ac.in

ABSTRACT

Damage accumulation during fatigue results in progressive stiffness degradation and alteration of dynamic characteristics in fibre-reinforced polymer composites. Employing such dynamic changes is a promising approach for structural health monitoring and predicting residual life. In this study, vibration-based fatigue life prediction of unidirectional glass fibre reinforced polymer (GFRP) laminates is investigated through experimental modal analysis combined with semi-empirical and machine learning models. Five GFRP specimens were fabricated and subjected to tensile, fatigue, and modal interrupted fatigue testing. Natural frequencies of the first six vibration modes were measured at different fatigue damage levels. Existing stiffness degradation models were transformed into frequency-based prediction models using the analytical relationship between stiffness degradation and natural frequency. Semi-empirical models proposed by Mao and Wu were fitted using the experimental data and validated by predicting the fatigue life of an unseen specimen. In parallel, support vector regression (SVR) and Gaussian process regression (GPR) models were developed using normalised modal frequencies as input features, where four specimens were used for training and one specimen for validation. Both single-mode and multi-mode prediction frameworks were developed to evaluate the effect of modal feature selection on prediction accuracy. Results indicate that higher modes exhibit greater sensitivity to fatigue damage, with Mode 4 providing the most reliable predictions. Among machine learning approaches, the single-mode GPR (GPR-S) model achieved the best predictive performance with a coefficient of determination (R^2) of 0.845 and a relative error (RE) of 17.57%. The semi-empirical Mao model demonstrated superior prediction capability with significantly lower relative error (2.88%), even with the truncated fatigue data. The study highlights that modal feature sensitivity plays a more critical role than algorithm complexity and demonstrates that integrating modal analysis with physics-based and data-driven approaches provides a reliable framework for residual fatigue life prediction of composite structures.

Keywords: residual life prediction, support vector regression, gaussian process regression, machine learning, structural health monitoring, GFRP composite

INTRODUCTION

Fibre-reinforced polymers (FRP) are widely employed in many industrial structures, such as aerospace, marine, and civil engineering, due to their high specific strength, high specific stiffness, and corrosion resistance [1–2]. Among them, Glass fibre reinforced polymers (GFRP) are extensively employed in load-carrying applications. When these structures are exposed to fatigue loading, due to progressive damage accumulation, the structure will start to lose its stiffness progressively, and ultimately lead to final failure [3–6]. Unlike metals, the fatigue degradation in composites is highly complex due to its damage mechanisms such as matrix cracking, fibre-matrix debonding and delamination [7–8]. Therefore, accurate evaluation of structural degradation is essential to ensure the reliability and integrity of the composite structures during service. Monitoring the evolution of damage and estimating the residual life of the structure is an important research problem in structural health monitoring (SHM) [9]. Conventionally, the fatigue life estimation was carried out with stress-life curves and a residual stiffness degradation model obtained through extensive experimental fatigue testing [10–11]. The disadvantages of these approaches are the requirement of large experimental datasets and the inability to provide real-time information about the structural condition during service. As a solution for this, vibration-based SHM techniques gained considerable attention from the research community [12]. These techniques exploit dynamic properties of the structure, such as natural frequencies, to assess the condition of the structure because these dynamic properties are directly influenced by the stiffness changes induced by fatigue damage [13].

Several studies have proven that natural frequency degradation can serve as an effective indicator of fatigue damage progression in composite structures [14]. When stiffness decreases due to fatigue damage accumulation, the natural frequency will also reduce according to the vibration theory. Therefore, by monitoring the modal frequency reduction, it is possible to interpret the damage state and estimate the residual life of the structure. Experimental modal analysis combined with fatigue testing has been used widely to establish the relationship between stiffness degradation and frequency reduction in composite structures [15]. To establish this relationship, semi-empirical stiffness models have been developed to describe the evolution of damage accumulation under fatigue loading [16]. Among them, the models proposed by Mao, Wu, Yang and Zhong are widely used formulations to represent the normalised stiffness as nonlinear functions of normalised fatigue life [13]. Mao et al. proposed an empirical fatigue damage model capable of capturing nonlinear stiffness degradation during cyclic loading [17]. Wu and Yao further improved this formulation by introducing parameters that account for different stages of fatigue damage evolution [18]. Similarly, Yang et al. developed a degradation model that incorporates nonlinear damage progression to represent stiffness reduction under fatigue loading conditions [19]. Zong and co-workers proposed another widely used formulation, which accurately represents stiffness degradation in composite laminates through normalised fatigue parameters [20]. Using the analytical relationship between stiffness and natural frequency, these models can be transformed into frequency-based residual life prediction models. Such physics-based models provide a practical approach to determine the residual fatigue life using vibration data. However, semi-empirical models primarily rely on predetermined functional forms and may not capture complex nonlinear degradation behaviour or specimen-to-specimen variability in experimental data entirely. With advances in technology, Machine learning (ML) methods emerged as a powerful tool for fatigue life prediction with an inherent nonlinear relationship and limited datasets [21-22]. Regression-based ML algorithms can learn structural response parameters and fatigue life relationships directly without explicit physical formulations [23]. Among various ML algorithms, support vector regression (SVR) and Gaussian process regression (GPR) have shown proven capabilities for problems with inherent data nonlinearity and limited data availability [24]. SVR provides a deterministic regression framework based on structural risk minimisation, and GPR offers a probabilistic approach capable of modelling prediction uncertainty [25]. Recent studies have explored alternative indicators for fatigue damage characterisation. For instance, Wojciech Macek et al. demonstrated that fractographic features such as fractal dimension can be correlated with crack initiation and fatigue life in metallic systems. Their work highlights the potential of measurable geometric descriptors to

infer fatigue damage history and structural degradation. Such approaches conceptually align with the present study, where modal frequency degradation is employed as a non-destructive indicator for fatigue damage progression [26].

Despite the increasing adoption of vibration-based structural health monitoring and machine learning techniques for fatigue life prediction of composite materials, several critical gaps remain in the existing literature [27]. First, most studies either focus on physics-based stiffness degradation models or purely data-driven machine learning approaches, with limited efforts toward a direct and systematic comparison using experimentally obtained modal degradation data. Second, although natural frequency reduction is widely recognised as an indicator of stiffness degradation, the explicit transformation of established stiffness-based fatigue models into frequency-based prediction frameworks has not been thoroughly validated using experimental fatigue-modal datasets. Third, the influence of modal order and the relative effectiveness of single-mode versus multi-mode vibration features in fatigue life prediction remain insufficiently explored, particularly under limited experimental data conditions.

To address these gaps, the present study proposes a comprehensive vibration-based fatigue life prediction framework integrating experimental modal analysis, semi-empirical degradation models and machine learning approaches. The fundamental novelty of this work lies in the unified integration of these components within a single experimental and analytical framework, enabling direct comparison and deeper insight into fatigue damage characterisation. The key contributions of this work are as follows: (i) transformation and validation of established stiffness degradation models into frequency-based fatigue life prediction models using experimentally measured modal data, (ii) development of a systematically acquired experimental dataset through fatigue interrupted modal testing of unidirectional GFRP laminates, (iii) detailed investigation of modal sensitivity across the first six vibration modes to identify the most informative damage sensitive features, (iv) comparative evaluation of single-mode and multi-mode machine learning frameworks (SVR and GPR) under limited data availability and (v) benchmarking of physics-based and machine learning models, demonstrating the relative effectiveness of modal feature selection over algorithm complexity in fatigue life prediction. Unlike existing studies that treat these approaches independently, the present work provides a consolidated framework that combines experimental validation, modal feature analysis, and model comparison, thereby offering new insights into the interplay between physical modelling and data-driven techniques for fatigue prognosis.

MATERIAL AND METHODS

Specimen fabrication

GFRP laminates were manufactured through the hand layup technique with S-glass fibre as reinforcement and epoxy matrix system (LY556 with HY951). The laminate stacking sequence is $[0°]_{10}$, representing a unidirectional configuration with ten plies aligned along the loading direction. Unidirectional laminates will result in fibre-dominated stiffness behaviour during fatigue and will establish a reasonable relationship between stiffness reduction and vibration behaviour under cyclic fatigue loading. During the process, the glass lamina was manually impregnated with epoxy matrix and stacked one over another to obtain the laminate in the form of a plate with the required thickness. The laminates were prepared over a flat mould and kept in the vacuum bagging to remove entrapped air and excess resin. Then the vacuum bagged plates are kept in a hot air oven at a curing temperature of 80 °C at a moderate heating rate for 3 hours to ensure the proper cross-linking of the epoxy matrix. Then the laminates were allowed to cool naturally inside the oven to room temperature to reduce the residual stresses. Then, specimens with dimensions of 250 × 25 × 2 mm were taken out along the fibre direction from the cured plates in accordance with the ASTM standards for tensile and fatigue testing, as shown in Figure 1. Edges of the specimens were deburred and sanded to minimise the machining-induced damage. Material characteristics and specimen configuration were summarised in Table 1.

Experimental procedures

Composite samples were used for tensile testing in accordance with ASTM D3039 and for fatigue testing in accordance with ASTM D3479. Further, they were utilised for modal and fatigue-interrupted modal testing.

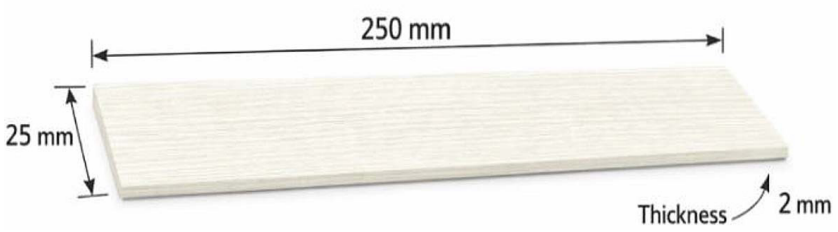

Figure 1. Specimen geometry used for experimental testing of unidirectional GFRP laminates

Table 1. Summary of material characteristics, specimen configuration, and fatigue test parameters

S. No	Parameter	Description	S. No	Parameter	Value
1	Fiber type	S-glass	8	Loading type	Tension–Tension
2	Matrix	Epoxy (LY556 & HY951)	9	Maximum stress	0.8 × σult
3	Stacking sequence	$[0°]_{10}$	10	Stress ratio	0.05
4	Specimen dimensions	250 × 25 × 2 mm^3	11	Frequency	5 Hz
5	Fibre volume fraction	55%	12	Waveform	Sinusoidal
6	Fabrication method	Hand layup with vacuum bagging	13	Environment	Room temperature and ambient humidity
7	Curing condition	80 °C for 3 hours	14	Run-out limit	10^6 cycles

Tensile testing

Tensile testing was performed to determine the ultimate tensile strength (σ_{ult}) of the specimens, which will be used to define maximum stress (σ_{max}) in the fatigue test and elastic modulus (E), which will be used as the initial stiffness (E_0) while establishing the stiffness vs natural frequency relationships. Tensile tests were carried out on a servo-hydraulic universal testing machine at a constant displacement rate of 2 mm/min until failure, as illustrated in Figure 2.

Fatigue testing

Tension-Tension fatigue testing was executed in the universal testing machine by keeping the maximum stress as 0.8 times the ultimate tensile strength of the specimen and the stress ratio R as 0.05, as shown in Figure 3. These fatigue parameters were chosen to ensure fibre-dominated failure and low-cycle fatigue behaviour. Loading was given in sine waveform with a 5 Hz frequency to minimise self-heating, and the run-out time was kept at 10^6 cycles**.** All experiments were conducted under laboratory ambient conditions (room temperature and humidity), without controlled environmental variation. These tests were conducted to obtain the fatigue life (N) of the composite specimens. Fatigue testing conditions were summarised in Table 1.

Modal testing

Modal testing was conducted on the composite specimens to determine their first six natural frequencies under fixed-free boundary conditions, as shown in Figure 4. The first six bending modes of the beam were illustrated in Figure 5. A single-axis accelerometer and data acquisition system (DAS) with an impact hammer was used to perform the single-input single-output experimental modal analysis through multi-point excitation to obtain the natural frequencies of higher modes. A piezoelectric accelerometer with sensitivity 100 mV/g was placed near the free end of the cantilever beam and considered as the reference measurement point with optimal sensitivity for all the modes. Beam was excited with an impact hammer with a force transducer tip, and both the sensor and accelerometer are connected to the data acquisition system. Grid points for excitation were marked at 12 equidistant locations along the beam length. Sampling frequency and frequency resolution were chosen as 10 kHz and 0.6 Hz, respectively. The resulting Frequency Response Functions were post-processed to obtain the natural frequencies. The analysis was limited to the first six vibration modes, as these modes exhibited clear and well-separated peaks with a high signal-to-noise ratio and good repeatability across specimens. Higher modes were not considered due to reduced

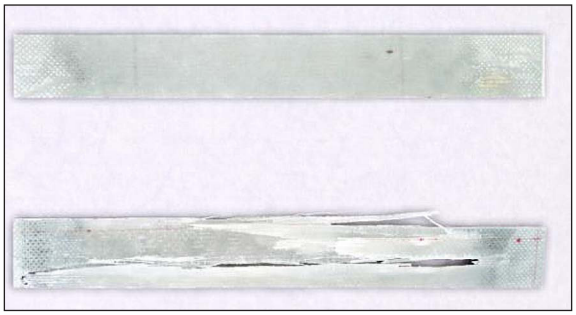

Figure 2. GFRP specimen used in tensile testing, and the specimen after tensile failure

response amplitude, increased modal overlap, and higher measurement uncertainty, which can affect reliable frequency identification. Furthermore, the experimental setup, involving single-axis acceleration measurement under transverse excitation, predominantly captured bending modes, while torsional modes were not distinctly excited or measured. Since bending modes are more sensitive to stiffness degradation in unidirectional laminates under tensile fatigue loading, the first six bending modes were considered sufficient for the present analysis.

Figure 3. Fatigue testing setup for tension–tension fatigue loading

Modal testing under fatigue damage

Fatigue testing and modal testing were performed sequentially on the GFRP laminates to establish the relationship between the stiffness reduction due to fatigue and the corresponding vibrational response in terms of natural frequencies. After the specific fatigue cycles, the specimens were taken out of the fatigue machine and tested for natural frequencies. The intervals had arrived from the fatigue life (N) of specimens obtained from the fatigue test. This test resulted in multiple datasets correlating the normalised fatigue life (n/N) with the normalised natural frequency (f_n/f_0). Where n is the actual fatigue cycle, f_n is the natural frequency after n fatigue cycles, and f_0 is the natural frequency of the undamaged specimen. To ensure consistency across specimens and enable direct comparison of modal degradation behaviour, a common fatigue interruption schedule was adopted for all specimens as shown in Table 0. The interruption points were defined based on the logarithmic mean fatigue life ($N = 7.26 \times 10^3$ cycles), which represents the central tendency of the fatigue life distribution. Fatigue tests were interrupted at predefined cycle intervals (0, 500, 1000, 1500, 2000, 2500, 3000, 3500, 4000, and 5000 cycles), corresponding to normalised fatigue life fractions (n/N) as shown in Table 2. At each interruption point, modal testing was performed on all five specimens and repeated five times for each case, resulting in multiple measurements capturing specimen-to-specimen variability. This approach ensured uniform sampling of fatigue degradation across all specimens while maintaining statistical representation of variability. Specimens were re-mounted using the same clamping configuration for each modal test. Care was taken to maintain consistent boundary conditions across repeated measurements. The overall methodology used here

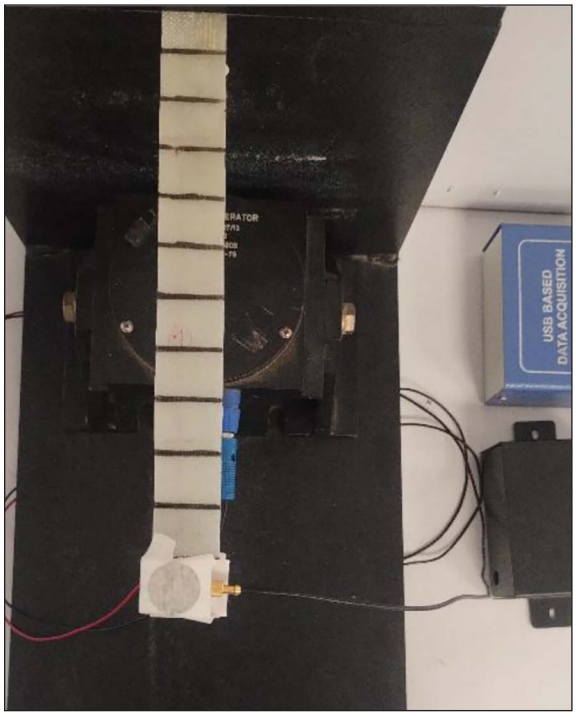

Figure 4. Modal testing setup of GFRP beam under fixed–free boundary conditions

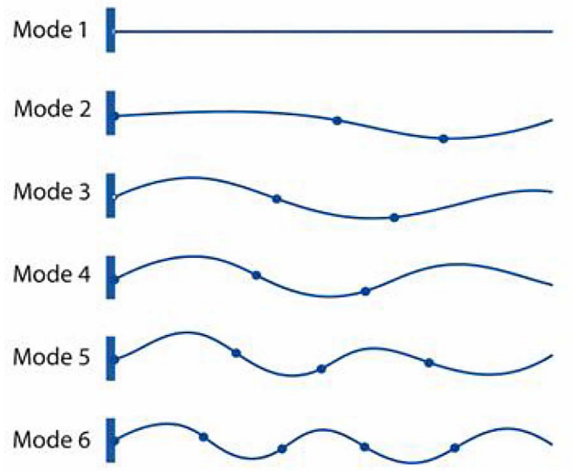

Figure 5. First six mode shapes of the specimen under fixed–free boundary conditions

for the fatigue life prediction using experimental modal analysis data through semi-empirical and machine learning techniques was illustrated using Figure 6.

Semi-empirical fatigue prediction models

Semi-empirical models proposed by Mao and Wu are used here to determine the residual fatigue life of unidirectional composite specimens based on the natural frequencies obtained.

Table 2. Fatigue interruption and modal measurement protocol

Interruption index	Fatigue cycles (n)	Normalised life (n/N)	No. of modal measurements
1	0	0.00	5
2	500	0.069	5
3	1000	0.138	5
4	1500	0.207	5
5	2000	0.275	5
6	2500	0.344	5
7	3000	0.413	5
8	3500	0.482	5
9	4000	0.551	5
10	5000	0.689	5

Through the analytical relationship between stiffness and natural frequency, the formulation was derived from existing stiffness degradation models. Various progressive damage mechanisms, such as delamination, debonding, etc., resulted in composite laminates due to fatigue loading, collectively degrading the longitudinal static stiffness of the composite laminates. Hence, the relationship between static stiffness and natural frequency can be exploited to quantify the extent of fatigue damage.

For a composite specimen, vibrating in bending, the natural frequency f can be expressed as:

$$f = \frac{k}{2\pi}\sqrt{\frac{EI}{\rho AL^4}} \tag{1}$$

where: E is the longitudinal modulus, I is the moment of inertia, ρ is the density, A is the cross-sectional area, L is the length, and k is the modal constant.

Rearranging Equation 1, the relationship between the stiffness and natural frequency can be expressed as:

$$E \; \alpha \; f^2 \tag{2}$$

Thus, the normalised stiffness degradation can be written in terms of normalised natural frequency as:

$$\frac{E_n}{E_0} = \frac{f_n^2}{f_0^2} \tag{3}$$

where: E_n is the stiffness of the specimen after n cycles.

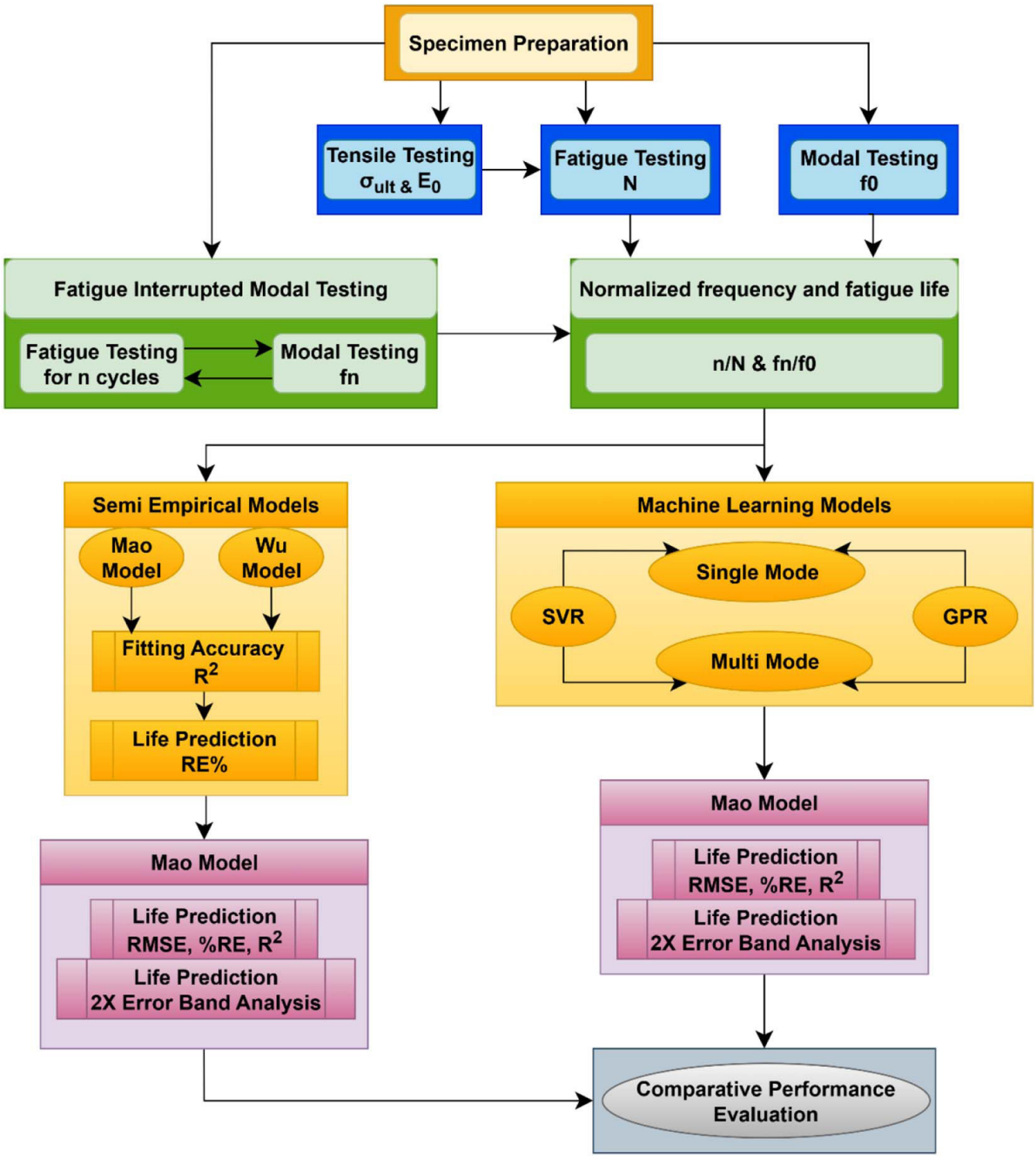

Figure 6. Overall framework for vibration-based fatigue life prediction integrating experimental modal analysis, semi-empirical models and machine learning techniques

This relationship helps to transform the existing residual stiffness models into frequency-based residual life prediction models.

Mao model

The residual stiffness model developed by Mao describes the normalised stiffness as a nonlinear function of normalised fatigue life:

$$\frac{E_n}{E_0} = 1 - \left[q \left(\frac{n}{N}\right)^a + (1-q)\left(\frac{n}{N}\right)^b \right] \quad (4)$$

where: q, a and b are the material-dependent constants [17].

Substituting Equation 3 into Equation 4, the frequency-based Mao model for predicting residual fatigue life becomes:

$$\frac{f_n^2}{f_0^2} = 1 - \left[q \left(\frac{n}{N}\right)^a + (1-q)\left(\frac{n}{N}\right)^b \right] \quad (5)$$

The unknown parameters q, a and b from the Mao model can be evaluated through nonlinear

regression using the experimental modal fatigue testing data.

Wu model

The model proposed by Wu expresses normalised stiffness as:

$$\frac{E_n}{E_0} = 1 - \left(1 - \frac{E_N}{E_0}\right)\left\{1 - \left[1 - \left(\frac{n}{N}\right)^b\right]^a\right\} \quad (6)$$

Using the stiffness frequency relationship Equation 3, the frequency-based Wu model for predicting residual fatigue life can be written as:

$$\frac{f_n^2}{f_0^2} = 1 - \left(1 - \frac{f_N^2}{f_0^2}\right)\left\{1 - \left[1 - \left(\frac{n}{N}\right)^b\right]^a\right\} \quad (7)$$

where: E_N is the stiffness of composite specimens just before the final failure, f_N is the natural frequency of composite specimens just before the final failure, and a and b are the material-dependent constants [18].

The unknown parameters a and b from the Wu model can be evaluated through nonlinear regression using the experimental modal fatigue testing data.

The increased sensitivity of higher vibration modes to fatigue-induced damage can be explained by structural dynamics principles. For a beam-like structure, the natural frequency is governed by the flexural stiffness EI, and the modal response is strongly influenced by the curvature of the mode shapes. The bending strain energy density is proportional to the square of curvature, $\kappa(x) = \frac{d^2\phi(x)}{dx^2}$, such that

$$U_i \, \alpha \int_0^L EI(x)\left(\phi_i''(x)\right)^2 dx \quad (8)$$

where: $\phi_i(x)$ is the ith mode shape.

Higher modes exhibit increased curvature and a larger number of inflexion points, leading to stronger localisation of modal strain energy. Consequently, a local reduction in stiffness $EI(x)$ due to fatigue damage produces a larger perturbation in the modal strain energy and, therefore, a more pronounced shift in natural frequency for higher modes.

From the first-order eigenvalue perturbation, the fractional frequency change can be approximated as:

$$\frac{\Delta f_i}{f_i} \approx -\frac{1}{2}\frac{\int_0^L \Delta EI(x)\left(\phi_i''(x)\right)^2 dx}{\int_0^L EI(x)\left(\phi_i''(x)\right)^2 dx} \quad (9)$$

indicating that frequency sensitivity is governed by the overlap between the damage-induced stiffness reduction ΔEI(x) and the curvature-squared field of the mode. Because $\left(\phi_i''(x)\right)^2$ is larger and more spatially varied for higher modes, the overlap integral increases, enhancing damage sensitivity. In addition, higher modes tend to exhibit modal strain energy localisation near regions of maximum curvature (often away from nodes), making them more responsive to localised damage such as matrix cracking, debonding, or delamination. However, this increased theoretical sensitivity is accompanied by reduced vibration amplitude and greater susceptibility to measurement noise and modal overlap at higher frequencies, which can limit practical identification accuracy. This explains why intermediate modes (e.g., mode 4 in the present study) provide an optimal balance between damage sensitivity and measurement reliability.

A portion of the experimental dataset was used for model fitting, and the remaining data will be used for validation. The goodness of fit is evaluated using the coefficient of determination R^2. After validation, the inverse form of the models was used to predict the fatigue life N based on measured frequencies.

Machine learning framework

Semi-empirical models described here to capture the stiffness degradation during fatigue rely primarily on the predetermined functional forms. They may not fully capture the specimen variability or nonlinearity in the degradation. ML algorithms are proposed here to improve prediction capability by directly establishing the nonlinear relationship between the measured natural frequencies and remaining fatigue life.

SVR and Gaussian process regression are the two ML algorithms adopted here for the study. The experimental dataset obtained from fatigue-interrupted modal testing was divided into training and validation sets, where data from Specimens 1–4 were used for training, and Specimen 5 was used for independent validation. This specimen-wise split was adopted to evaluate the predictive capability of the models on an unseen specimen and to

reflect realistic fatigue life prediction conditions. The input features, the normalised squared frequency ratios (f_n^2/f_0^2) and the output variable, normalised fatigue life (n/N), was scaled using min–max normalization within the range [0,1]. The normalisation parameters were determined using only the training dataset and subsequently applied to the validation dataset to avoid data leakage.

Support vector regression (SVR) model

SVR is a supervised ML algorithm highly suitable for nonlinear regression problems. It is highly effective for problems associated with minimum datasets due to its structural risk minimisation principle. For the SVM model, a radial basis function (RBF) kernel was employed to capture nonlinear relationships. The hyperparameters were selected through systematic tuning within the following ranges:

- $C \in [1, 10, 100, 1000]$
- $\gamma \in [0.01, 0.1, 1, 1000]$

The final model parameters were chosen based on the best predictive performance on the validation dataset.
Given a training dataset:

$$\{(x_i, y_i)\}, i = 1,2,3, \ldots\ldots, n \qquad (10)$$

where: x_i is the input vector, here the normalised natural frequency, and y_i is the Normalized fatigue life.

The SVR regression function is:

$$f(x) = w \cdot \phi(x) + b \qquad (11)$$

where: $\phi(x)$ is the nonlinear mapping to high-dimensional feature space, w is the weight vector, and b is the bias term.

The optimisation objective minimises as shown in Equation 12, subject to the ε-insensitive loss constraints.

$$\frac{1}{2}\|w\|^2 + C\sum_{i=1}^{n}\left((\xi_i + \xi_i^*)\right) \qquad (12)$$

RBF kernel was adopted to capture nonlinear behaviour as shown in Equation 13.

$$K(x_i, x_j) = exp\left(-\gamma\|x_i - x_j\|^2\right) \qquad (13)$$

where: C is the penalty parameter, and γ is the kernel parameter.

After training, the SVR algorithm predicts the normalised fatigue life based on the measured frequency input and then the predicted life is converted into actual fatigue cycle counts. SVR provides a deterministic nonlinear regression baseline for comparison with both probabilistic ML and physics-based models.

Gaussian process regression (GPR) model

Gaussian Process Regression is a probabilistic, nonparametric regression technique that is well-suited for problems with minimal datasets available for training. Unlike deterministic models, GPR does mean predictiona as well as uncertainty estimation, which are very much required for problems like fatigue life prediction where data variability is high. For the GPR model, a RBF kernel was used. The hyperparameters, including signal variance (σ_f^2) and characteristic length scale (l), were optimised automatically during training using maximum likelihood estimation.

In GPR, the regression function is assumed as shown in Equation 14 to follow a Gaussian process.

$$f(x) \sim GP\big(m(x), k(x, x')\big) \qquad (14)$$

where: $m(x)$ is the mean function and $k(x, x')$ is the covariance function.

In this problem, with normalisation, the mean function was assumed to be zero. Using a squared exponential kernel, the covariance was modelled as:

$$k(x_i, x_j) = \sigma_f^2 exp\left(-\frac{\|x_i - x_j\|^2}{2l^2}\right) \qquad (15)$$

where: σ_f^2 is the hyperparameter signal variance and l is the characteristic length scale.

These hyperparameters are optimised during training by maximum likelihood estimation. For a new input x*, the GPR results in a predictive mean μ* and a predictive variance σ^{*2}. This predictive variance enables quantification of uncertainty bounds in fatigue life estimation. The predicted fatigue life was taken as the predictive mean, and confidence intervals were constructed using the predictive variance.

All computations were performed using Python. A fixed data split and consistent preprocessing procedure were maintained throughout the study to ensure reproducibility of the

results. Due to the limited size of experimentally obtained fatigue datasets, a specimen-wise validation approach was preferred over random data splitting, ensuring that model evaluation reflects practical fatigue life prediction scenarios.

EXPERIMENTAL RESULTS

Tensile properties

Five valid specimens with failure at the gauge length were taken for consideration, and their mean Elastic modulus and Tensile strength, along with standard deviation, are reported here in Table 3. Tensile characterisation of GFRP laminates with elastic modulus 30.1 ± 0.9 GPa indicates a narrow dispersion, uniform load transfer along the principal fibre direction. Similarly, the ultimate tensile strength 479 ± 20 MPa reflects low variability with consistent fibre-dominated mechanical performance. Low standard deviation in stiffness and tensile strength results is important for the fatigue life prediction studies. Since frequency-based residual life prediction models heavily rely on stiffness degradation, low variability ensures the measured frequency changes are primarily due to the fatigue damage degradation.

Fatigue life characteristics

Tension-Tension fatigue tests are conducted with stress ratio R = 0.05 and $\sigma_{max} = 0.8^* \sigma_{ult}$ as shown in Table 4. Statistical descriptors and the observed cycles to failure of five valid specimens are reported in Table 5.

Results of fatigue life show substantial scatter with more than one order of magnitude, which is characteristic of unidirectional GFRP under high stress amplitude fatigue. The failure is governed by stochastic fibre fracture and localised damage accumulation. Under the stated loading conditions, the fatigue damage is fibre-dominated with rapid stiffness degradation. Low fatigue life resulted from certain specimens, confirming that the high stress level produces accelerated damage progression, making this condition suitable for the investigation of frequency-based residual life. Further, fatigue variability directly affects the predictive accuracy of machine learning models. Hence, robust validation strategies are essential for realistic prediction capability.

From the fatigue life data and statistical descriptors shown in Table 5, the statistical descriptors indicate significant scatter in fatigue life, with a coefficient of variation greater than unity. Hence, a consistent value of fatigue life N is required for further investigation. Since the fatigue life of GFRP laminates follows a log-normal distribution, statistical evaluation of the mean logarithmic fatigue life was performed, and the result was N = 7.26 × 10^3 cycles

This gives a more representative central tendency than the arithmetic mean due to the presence of high-life outliers. Fatigue life data were analysed on a logarithmic scale due to their inherent statistical characteristics. Fatigue life typically follows a log-normal distribution and spans multiple orders of magnitude, making direct averaging in the linear scale less representative. In addition, linear averaging is sensitive to extreme values or outliers, which can disproportionately influence the mean fatigue life. Logarithmic transformation reduces this bias, stabilises variance, and provides a more meaningful and consistent representation of fatigue behaviour.

Modal degradation behaviour

The first six natural frequencies of the specimens were measured in an undamaged state as well as at predefined fatigue intervals under fixed free boundary conditions. For each case, five data sets were recorded to account for the specimen-to-specimen variability and measurement noise. In general, GFRP laminates showed a progressive reduction in natural frequencies and stiffness with increasing fatigue cycles due to accumulated fatigue damage. The natural frequency degradation with increasing fatigue cycles is evident across all modes and specimens. The rate of reduction varied among specimens and modes. Figure 7 shows

Table 3. Mechanical properties of unidirectional GFRP laminates from tensile testing

Parameter	Mean	Standard deviation
Longitudinal elastic modulus E in GPa	30.1	0.9
Ultimate tensile strength σ_{ult} in MPa	479	20

Table 4. Loading parameters used for fatigue testing of unidirectional GFRP laminates

R	σ_{max}	σ_{max} in MPa	σ_{min} in MPa	σ_{mean} in MPa	σ_{amp} in MPa
0.05	0.8* σult	383.2	19.16	201.18	182.02

Table 5. Fatigue life of unidirectional GFRP specimens under tension–tension cyclic loading and statistical descriptors

Specimen	1	2	3	4	5
Fatigue life in cycles	1.9 × 10^3	1.1 × 10^4	6.3 × 10^3	3.4 × 10^3	4.5 × 10^4
S. No	Statistical descriptor		Value		
1	Arithmetic mean (cycles)		13520		
2	Standard deviation (cycles)		17934		
3	Coefficient of variation		1.33		
4	Logarithmic mean (cycles)		7260		

the natural frequency degradation as a function of fatigue cycles for the first six bending modes of GFRP laminate specimens. The plots represent interrupted modal measurements obtained during fatigue testing for five specimens.

To evaluate the repeatability of modal measurements, multiple undamaged specimens were tested under identical clamping conditions. The variation in measured natural frequencies was quantified in terms of standard deviation and coefficient of variation (CoV) as summarised in Table 6. The results indicate that the CoV remains approximately 1% for all considered modes, demonstrating good repeatability of the experimental setup. The observed uncertainty is significantly lower than the frequency shifts induced by fatigue damage, ensuring reliable damage characterisation. Special care was taken to maintain consistent clamping conditions by using a rigid fixture and a controlled tightening procedure to minimise boundary condition variability.

In mode 1, the natural frequency of the undamaged specimen varies between 20.89 Hz and 23.18 Hz, which shows acceptable variation due to fabrication and clamping conditions. Further, it reduced between 17.95 Hz and 19.87 Hz at 5000 cycles with a gradual decline in between. The reduction varies approximately 10 to 20% between the specimens. Some minor non-monotonic fluctuations were also observed at intermediate cycles due to experimental uncertainty and clamping effects.

In mode 2, the specimens showed a consistent decreasing trend in natural frequencies from 141.51 to 146.89 Hz at zero cycles to 116.04 to 123.54 Hz at 5000 cycles. Overall reduction in natural frequency from 0 cycles to 5000 cycles ranges from 14% to 19%. In specimen 4. Some intermediate cycle fluctuations were observed, likely due to modal interaction and variation in boundary stiffness.

Mode 3 exhibited a stronger degradation when compared to mode 1, and mode 2 ranged from 362.4 to 368.2 Hz at zero cycles to 276.3 to 304.3 Hz at 5000 cycles. The reduction ranged between 17 to 24%. A larger relative reduction of natural frequencies in mode 3 confirms the increased sensitivity of higher modes toward stiffness changes.

Table 6. Summary of modal measurement repeatability parameters

Mode	Mean frequency (Hz)	Std. Dev. (Hz)	CoV (%)
1	22.038	0.15–0.25	0.8–1.2
2	143.746	0.8–1.5	0.6–1
3	364.908	2–4	0.6–1
4	683.31	4–7	0.6–1
5	1093.9	6–10	0.5–0.9
6	1541.566	8–15	0.5–1

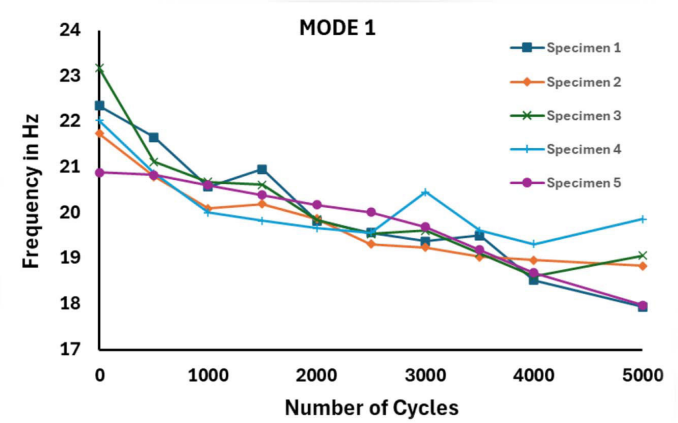
MODE 1
Frequency in Hz
Number of Cycles
Specimen 1
Specimen 2
Specimen 3
Specimen 4
Specimen 5
24
23
22
21
20
19
18
17
0
1000
2000
3000
4000
5000

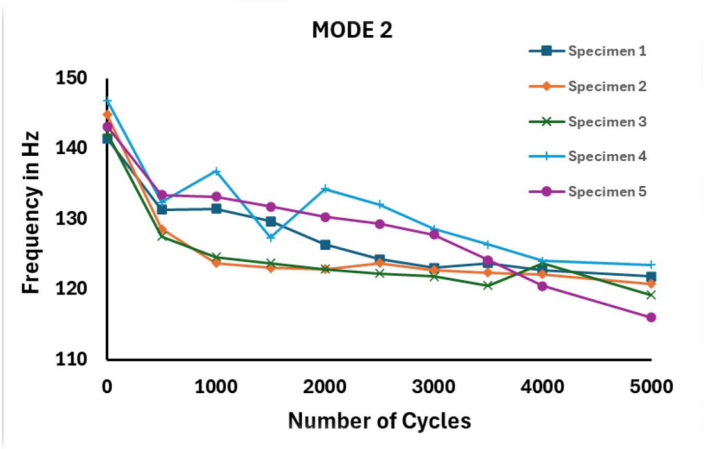
MODE 2
Frequency in Hz
Number of Cycles
Specimen 1
Specimen 2
Specimen 3
Specimen 4
Specimen 5
150
140
130
120
110
0
1000
2000
3000
4000
5000

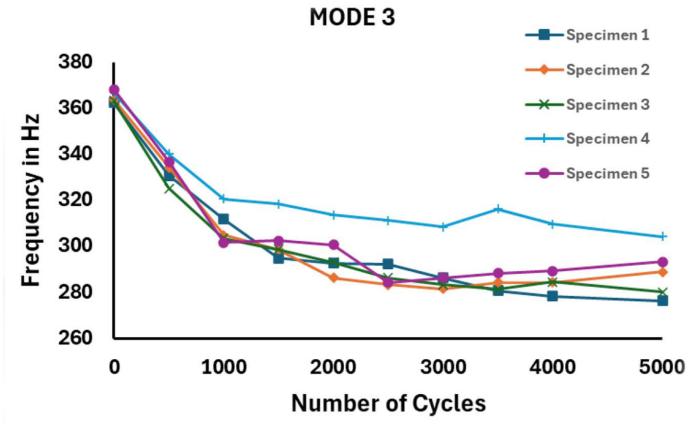
MODE 3
Frequency in Hz
Number of Cycles
Specimen 1
Specimen 2
Specimen 3
Specimen 4
Specimen 5
380
360
340
320
300
280
260
0
1000
2000
3000
4000
5000

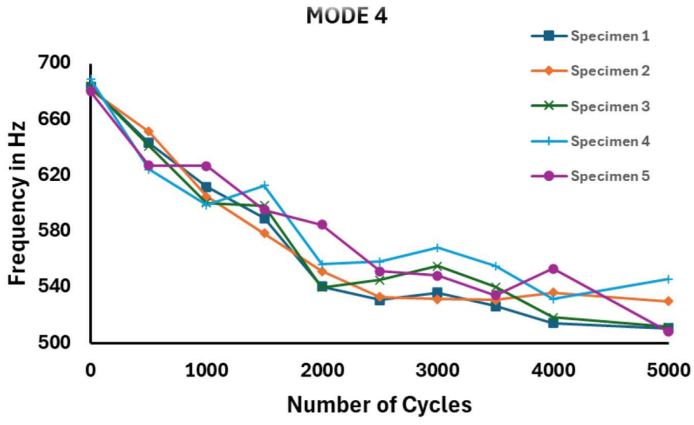
MODE 4
Frequency in Hz
Number of Cycles
Specimen 1
Specimen 2
Specimen 3
Specimen 4
Specimen 5
700
660
620
580
540
500
0
1000
2000
3000
4000
5000

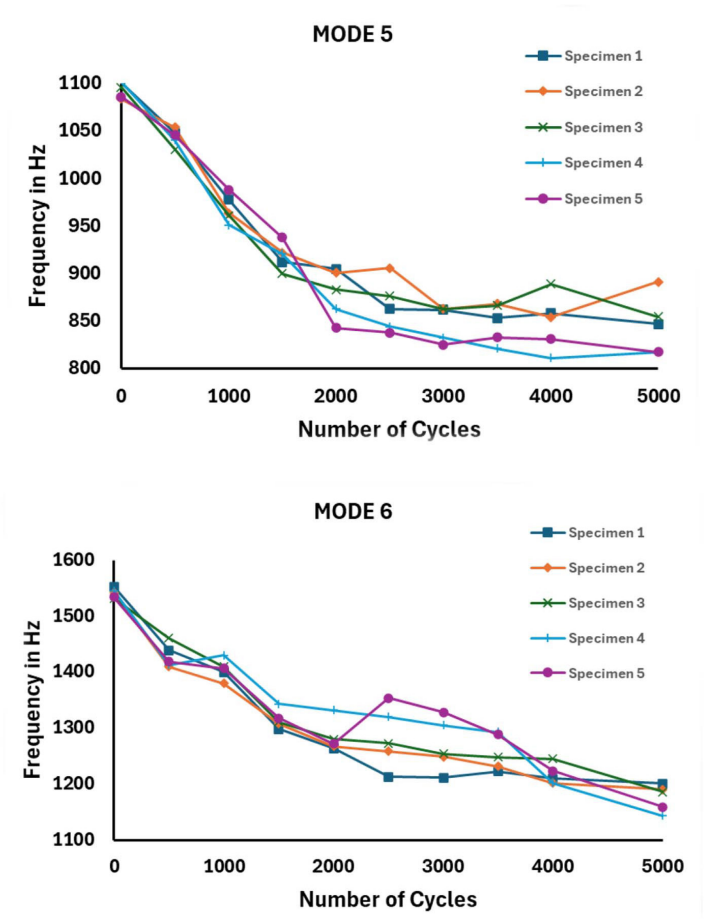

Figure 7. Natural frequency degradation with increasing fatigue cycles for the first six bending modes (MODE 1 to MODE 6) of cantilever GFRP specimens

Intermediate fluctuations are visible in specimen 4 and specimen 5, but the general trend remains decreasing.

Mode 4 resulted in a significant reduction in natural frequencies from 679.8 to 688.6 Hz at zero cycles to 508.3 to 545.8 Hz at 5000 cycles. The reduction observed was between 20 to 25%. The degradation shows increased scatter compared to lower modes, which resulted from higher mode sensitivity and the influence of excitation location. Slight peak broadening in FRFs is also noted during the testing. Despite these fluctuations, a clear overall reduction trend is observed.

Mode 5 natural frequency reduced from 1084.3 to 1101.7 Hz at zero cycles to 817.6 to 891.6 Hz at 5000 cycles. The reduction ranged between 18 to 25%. Some specimens, example specimen 2 and specimen 3, show localised frequency recovery at intermediate frequencies due to stiffness redistribution and higher frequency measurement sensitivity.

Mode 6 demonstrated the largest absolute reduction in natural frequency, varying from 1532.3 to 1553.3 Hz at zero cycles to 1143.6 to 1201.3 Hz at 5000 cycles. The reduction ranged between 22 to 26%. The more pronounced changes were observed because the higher bending modes are inherently more sensitive to local stiffness degradation. Large scatter at higher cycles is consistent with progressive damage accumulation and increasing structural nonlinearity.

Even though all six modes resulted in frequency degradation with fatigue progression, higher modes exhibited greater sensitivity to damage. Significant scatter was noted at higher fatigue cycles across all modes. Intermediate frequency recovery noticed at certain specimens across modes is within the acceptable tolerance. The progressive natural frequency reduction due to stiffness degradation ensures the suitability of vibration-based methods for fatigue life prediction models.

It should be noted that the present study infers fatigue damage progression indirectly

through changes in modal properties, without direct microstructural or fractographic characterisation. While vibration-based indicators provide a non-destructive and real-time assessment of structural degradation, they do not explicitly capture the underlying damage mechanisms such as matrix cracking, fibre breakage, or delamination. Therefore, the correlation between modal frequency reduction and internal damage evolution remains indirect. Future work may integrate vibration-based monitoring with direct damage characterisation techniques to establish a more comprehensive understanding of fatigue behaviour in composite structures.

Normalised frequency-life relationship

To provide direct representation of natural frequency degradation with respect to fatigue life, the natural frequencies and fatigue lives were normalised. This will remove the specimen-to-specimen variability across all six vibrational modes. Measured natural frequencies (fn) at different fatigue cycles (n) were normalised with respect to the natural frequency of undamaged specimens (f0) as shown in Figure 8. Similarly, the fatigue cycles (n) were normalised with respect to the mean logarithmic fatigue life (N). The resulted normalized frequency degradation ($0 \leq$ fn/f $0 \leq 1$) curves are presented as a function of normalised fatigue life ($0 \leq$ n/N ≤ 1).

At very initial stages (n/N<0.2) of fatigue life, all modes resulted in a relatively small degradation in natural frequencies. This indicates the early stiffness is primarily due to the matrix microcracking and localised fibre matrix debonding. In the intermediate (0.2< n/N<0.6) life regime, the frequency degradation was more severe, and it was found to be highly nonlinear in nature. This shows that during the intermediate life cycles, the stiffness loss increases progressively due to the accumulation of distributed damage and initiation of fibre breakage clusters. Close to the failure (0.6<n/N<0.7), the degradation rate reduced and beyond that, a sharp decline in the natural frequency will occur due to unstable damage growth and rapid loss of structural integrity before the final fracture. This behaviour aligns with the fatigue damage evolution in unidirectional GFRP laminates subjected to high stress amplitude loading.

Further, mode 1 resulted in the least reduction in normalised frequency, and higher modes exhibited larger degradation. This behaviour is consistent with vibration theory because the higher modes are more sensitive to the local stiffness variations. Small non-monotonic fluctuations were observed at intermediate fatigue lives primarily due to experimental uncertainty in peak identification, boundary condition variability during repeated clamping and modal coupling effects in higher frequency bands. However, the global decreasing trend ensures the applicability of the fatigue life degradation models.

FATIGUE LIFE PREDICTION RESULTS

Semi-empirical model performance

The nonlinear degradation trend across the vibration modes ensures the applicability of the Wu and Mao semi-empirical formulations. The collapse of normalised data into a bounded degradation region confirms that normalised frequency can serve as a reliable stiffness-based damage parameter. Furthermore, the modal dependency observed in the degradation rates suggests that higher modes may provide improved sensitivity for residual life prediction models. While employing the Wu and Mao models to fit the data, the fatigue cycle region 0 to 5000 will only be considered. Because at the N = 7260 cycles, the vibration data will have much higher scatter, and it is impractical to capture the experimental frequency just before the failure.

Model fitting accuracy

Experimentally obtained normalised natural frequency (f_n^2/f_0^2) versus normalised life (n/N) from specimens 1 to 4 were employed here to evaluate the unknown coefficients of the Mao and Wu frequency-based models. The quality of fitting of each model was assessed by determining the coefficient of determination using Equation 16 and is shown in Table 7.

$$R^2 = 1 - \frac{\sum(y_i - \hat{y}_i)^2}{\sum(y_i - \bar{y}_i)^2} \tag{16}$$

where: y_i – square ratio of normalised experimental frequency, $\hat{y}_i$ – model prediction, $\bar{y}_i$ – mean of experimental values.

The fitting performance of both models improves progressively with an increase in mode numbers. Mode 1 shows the poor correlation due

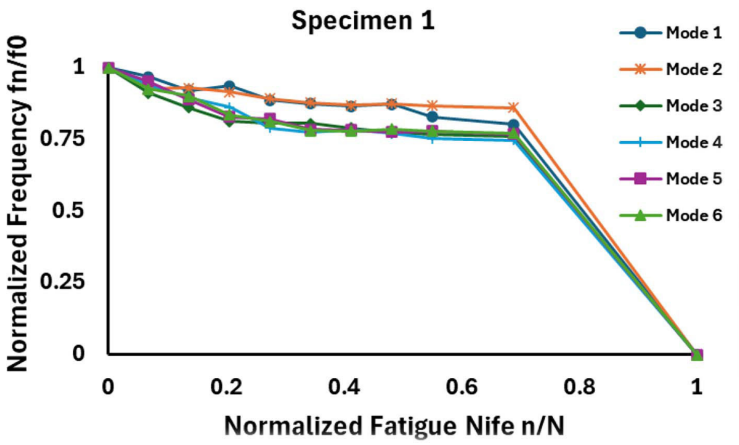
Specimen 1
Normalized Frequency fn/f0
Normalized Fatigue Nife n/N
Mode 1
Mode 2
Mode 3
Mode 4
Mode 5
Mode 6
0
0.25
0.5
0.75
1
0.2
0.4
0.6
0.8

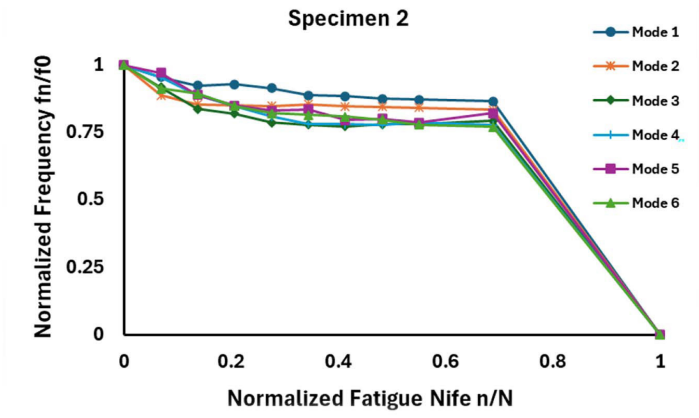
Specimen 2
Normalized Frequency fn/f0
Normalized Fatigue Nife n/N
Mode 1
Mode 2
Mode 3
Mode 4
Mode 5
Mode 6
0
0.25
0.5
0.75
1
0.2
0.4
0.6
0.8

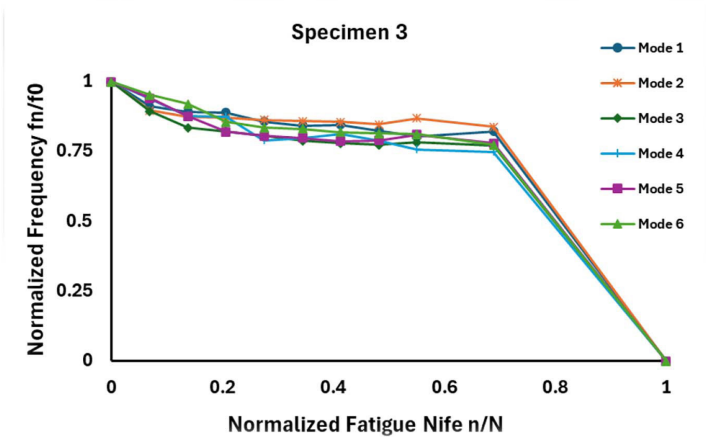
Specimen 3
Normalized Frequency fn/f0
Normalized Fatigue Nife n/N
Mode 1
Mode 2
Mode 3
Mode 4
Mode 5
Mode 6
0
0.25
0.5
0.75
1
0.2
0.4
0.6
0.8

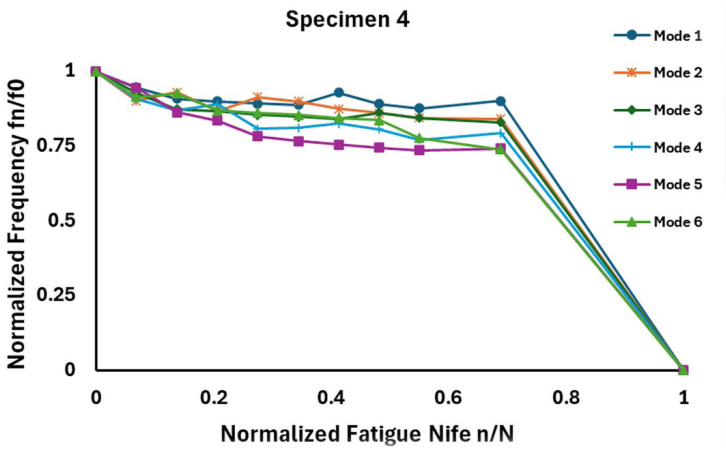
Specimen 4
Normalized Frequency fn/f0
Normalized Fatigue Nife n/N
Mode 1
Mode 2
Mode 3
Mode 4
Mode 5
Mode 6
0
0.25
0.5
0.75
1
0.2
0.4
0.6
0.8

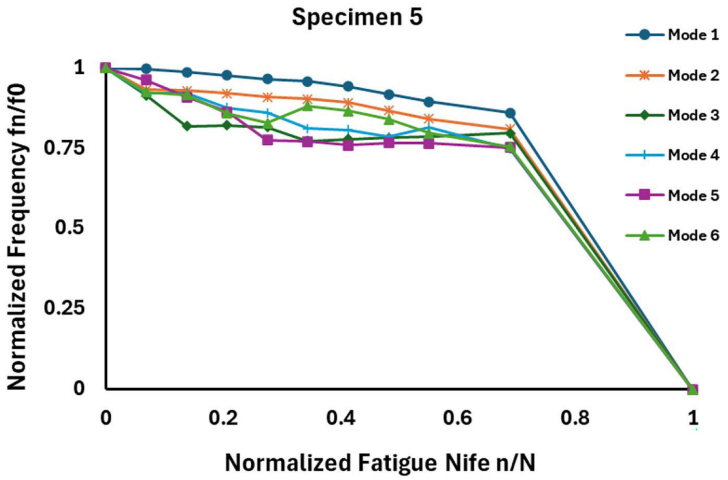

Figure 8. Normalised natural frequency degradation (f_n/f_0) as a function of normalised fatigue life (n/N) for the six vibration modes of GFRP specimens (Specimen 1 to Specimen 5)

to its boundary condition sensitivity and experimental noise. In contrast, the higher modes exhibit improved correlation through monotonic degradation trends. Mode 6 gives the highest fitting accuracy in both models, showing that the higher mode frequencies are more sensitive to the cumulative fatigue damage and stiffness degradation.

The fitted parameters of the Mao and Wu models obtained through nonlinear regression are summarised in Table 7. The results indicate that the Mao model parameters exhibit a systematic trend across different vibration modes, with the weighting factor q increasing and the exponents a and b decreasing with increasing mode number. This reflects a smoother and more stable representation of stiffness degradation in higher modes. The corresponding goodness-of-fit values show that the prediction accuracy improves significantly from Mode 1 to Mode 6, as indicated by increasing R^2 and decreasing RMSE values. In comparison, the Wu model parameters exhibit relatively less variation across modes, indicating limited flexibility in capturing nonlinear stiffness degradation behaviour. Consequently, the Wu model consistently shows slightly lower R^2 and higher RMSE values than the Mao model. This difference can be attributed to the dependence of the Wu model on terminal stiffness values, which introduces additional uncertainty when fatigue data is truncated. By using the power-type formulation, the Mao model captures the early to intermediate fatigue degradation well. This clearly indicates the usability of the Mao model in practical applications where the close failure data are not available and generally not useful. Whereas the Wu model that represents the two-stage degradation behaviour will require the data even in the late life regions for improved fitting performance. These results confirm that the Mao model provides a more robust and accurate representation of fatigue-induced stiffness degradation for the present dataset. Due to the limited size of the experimentally obtained fatigue dataset and the specimen-wise fitting approach, parameter confidence intervals were not evaluated. Instead, model robustness was assessed through goodness-of-fit measures (R^2 and RMSE) and validation performance on an independent specimen.

Residual analysis was performed using specimen-wise data from the training set (Specimens 1–4) to evaluate the fitting quality of the semi-empirical models. The residual plots, presented in Figure. 9, reveal that the Mao model produces a more consistent and uniformly distributed residual pattern centred around zero across all vibration modes. In contrast, the Wu model exhibits relatively higher scatter and noticeable deviation, particularly in the intermediate fatigue regime, indicating reduced capability in capturing nonlinear stiffness degradation behaviour. Furthermore, a progressive reduction in residual spread is observed from Mode 1 to Mode 6 for both models, confirming that higher vibration modes are more sensitive to fatigue-induced stiffness changes. This trend is consistent with the corresponding improvements in R^2 and RMSE values and reinforces the suitability of higher modal features for fatigue life prediction. Overall, the residual

Table 7. Fitted parameters and goodness of fit measures obtained from the nonlinear fitting of Mao and Wu semi-empirical models for different vibration modes

Mode	Mao model					Wu model			
	Parameters			R^2	RMSE	Parameters		R^2	RMSE
	q	a	b			a	b		
Mode 1	0.48	3.21	3.87	0.72	0.081	1.92	2.85	0.67	0.091
Mode 2	0.52	2.18	3.05	0.9	0.042	1.75	2.48	0.87	0.049
Mode 3	0.55	1.94	2.62	0.92	0.036	1.62	2.31	0.9	0.043
Mode 4	0.58	1.72	2.28	0.94	0.031	1.55	2.14	0.92	0.037
Mode 5	0.61	1.51	2.05	0.96	0.026	1.48	1.98	0.94	0.032
Mode 6	0.63	1.38	1.92	0.97	0.023	1.42	1.85	0.95	0.028

analysis provides strong evidence that the Mao model offers a more stable and accurate representation of stiffness degradation compared to the Wu model for the present experimental dataset. The residual distribution further demonstrates that model performance is governed not only by statistical indicators but also by the physical sensitivity of modal features to damage evolution.

Remaining fatigue life prediction

Fitted Mao and Wu semi-empirical models were validated using the data obtained from specimen 5, which was not taken into account for fitting. Experimentally measured normalised frequency ratio (f_n^2/f_0^2) was used as input to predict the normalised fatigue life. The accuracy of the prediction was assessed using a logarithmic relative error formulation using Equation 17 to account for the inherent log-normal distribution of composite fatigue life.

$$Relative\ Error\ RE = \\ = \frac{1}{m}\sum\left|\frac{log_{10}(N_{measured}) - \\ -log_{10}(N_{predicted})}{log_{10}(N_{measured})}\right| \quad (17)$$

where: m – Total number of predicted samples.

The results in Table 8 show that the prediction accuracy increases significantly with an increase in mode numbers. This confirms that the choice of modal order has higher significance than the semi-empirical models in prediction accuracy. Mode 1 resulted in the highest prediction error, about 30%, and this is due to the boundary clamping sensitivity and poor sensitivity to stiffness degradation. At higher modes, the prediction error significantly reduced due to improved monotonic degradation trend. Mode 4 shows the significant instability in prediction between the semi-empirical models due to truncated data availability. Two-stage degradation formulation used in the Wu model likely requires the end-of-life fatigue data to stabilize it prediction performance. On the other hand, the power law degradation formulation used in the Mao model effectively performs with early to mid-life fatigue data. The Mao model consistently outperformed the Wu model across all modes with practically possible truncated data sets, indicating its suitability for practical applications. The Wu model resulted in significant instability, particularly in mode 4 and mode 5, in prediction due to the non-availability of end-of-life degradation data.

Error band analysis

Using the parameters obtained through nonlinear regression of experimental data, the 2-time error band analysis of the Mao semi-empirical model was performed. Specimen 5 was used as the validation specimen for performing the 2-time error band analysis to assess the robustness of the Mao model in remaining fatigue life prediction. Using numerical inversion of the Mao formulation, the predicted fatigue life $N_{Predicted}$ was calculated within the physically admissible range $0<n/N<1$ using squared normalised frequency. To maintain consistency with the fatigue life representation, the predicted and measured fatigue lives were converted to a logarithmic scale.

The 2-time error band plot in Figure 10 shows that most of the fatigue life values are within the bands. This indicates the prediction capability of the Mao model with truncated fatigue data sets. Mode 1 results in a large scatter from the

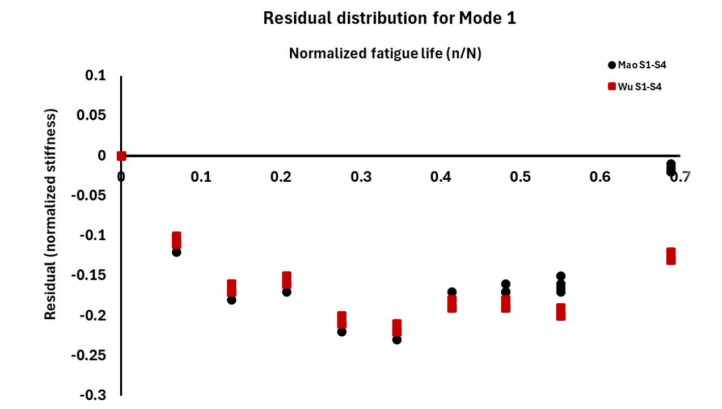
Residual distribution for Mode 1
Normalized fatigue life (n/N)
Mao S1-S4
Wu S1-S4
Residual (normalized stiffness)
0.1
0.05
0
-0.05
-0.1
-0.15
-0.2
-0.25
-0.3
0
0.1
0.2
0.3
0.4
0.5
0.6
0.7

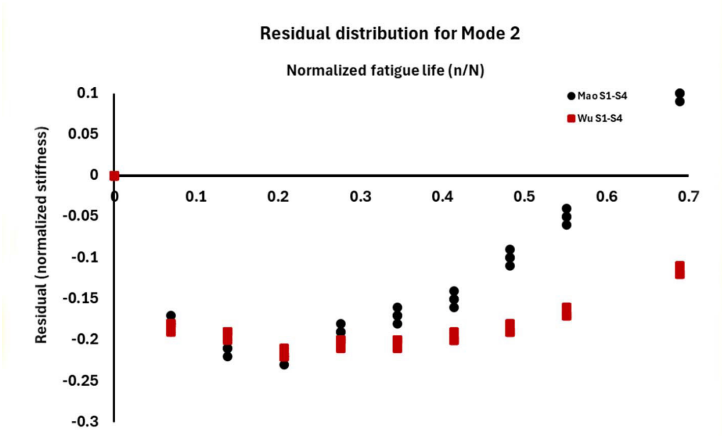
Residual distribution for Mode 2
Normalized fatigue life (n/N)
Mao S1-S4
Wu S1-S4
Residual (normalized stiffness)
0.1
0.05
0
-0.05
-0.1
-0.15
-0.2
-0.25
-0.3
0
0.1
0.2
0.3
0.4
0.5
0.6
0.7

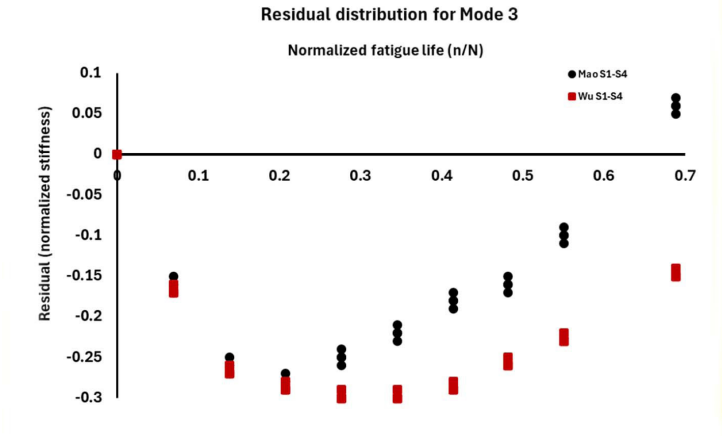
Residual distribution for Mode 3
Normalized fatigue life (n/N)
Mao S1-S4
Wu S1-S4
Residual (normalized stiffness)
0.1
0.05
0
-0.05
-0.1
-0.15
-0.2
-0.25
-0.3
0
0.1
0.2
0.3
0.4
0.5
0.6
0.7

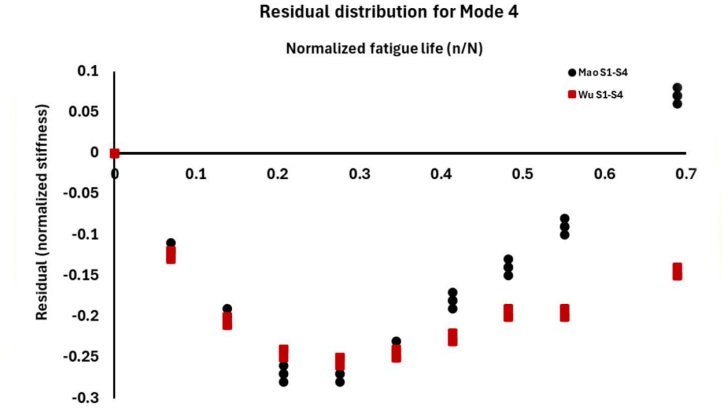
Residual distribution for Mode 4
Normalized fatigue life (n/N)
Mao S1-S4
Wu S1-S4
Residual (normalized stiffness)
0.1
0.05
0
-0.05
-0.1
-0.15
-0.2
-0.25
-0.3
0
0.1
0.2
0.3
0.4
0.5
0.6
0.7

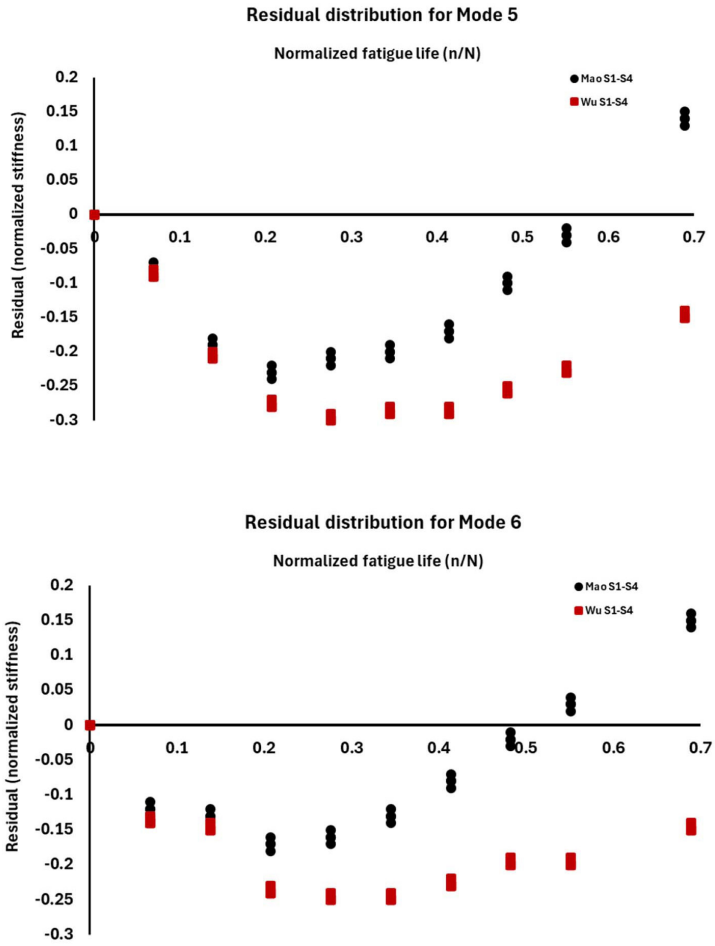

Figure 9. Residual plots of the Mao and Wu models for Modes 1–6 based on specimen-wise training data (specimens 1–4)

Table 8. Relative error (RE%) obtained for fatigue life prediction using Mao and Wu semi-empirical models for different vibration modes

Mode	Mao RE%	Wu RE%	Average RE%
Mode 1	29.97	9.22	19.595
Mode 2	13.31	9.22	11.265
Mode 3	6.46	9.24	7.85
Mode 4	2.88	19.13	11.005
Mode 5	7.48	10.23	8.855
Mode 6	6.88	9.22	8.05

prediction line, especially at lower measured lives. This clearly shows that the fundamental bending mode, primarily governed by global stiffness characteristics and small variations in frequency, leads to amplified uncertainty during inverse operations. Mode 2 and Mode 3 demonstrate intermediate scatter, and more points are clustered around the prediction line. This reduction in dispersion suggests the improved sensitivity to accumulated stiffness degradation. Higher modes resulted in the most stable behaviour, and their prediction was closely aligned with the prediction line across the measured fatigue life range. Some minor deviations are observed at lower fatigue cycles, but no systematic bias was observed. This shows the robustness of the Mao model in estimating the residual fatigue life.

Machine learning model performance

To assess the capability of machine learning-based fatigue life prediction models, four machine learning frameworks are implemented and systematically compared. Those are single-mode support vector regression (SVR-S), single-mode Gaussian process regression (GPR-S), multi-mode support vector regression (SVR-M) and multi-mode Gaussian process regression (GPR-M). All the models were trained with the experimentally

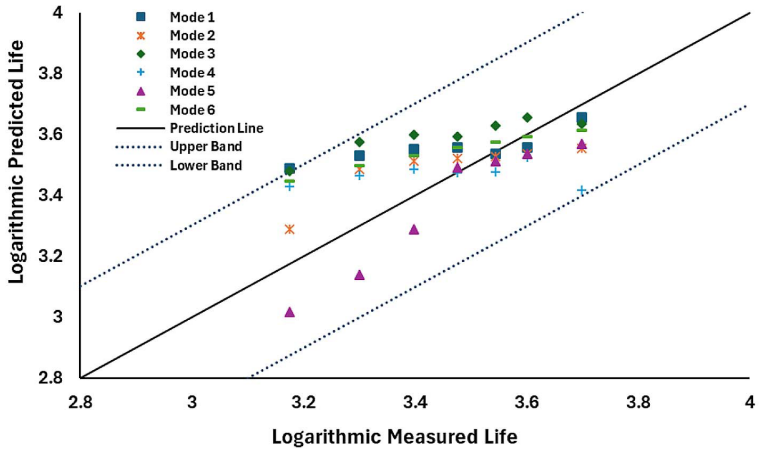

Figure 10. Two-times error band analysis for fatigue life prediction using the Mao semi-empirical model based on normalised modal frequency degradation

obtained model degradation data and validated using an unseen specimen. Normalised squared frequency ratios are given as input futures, and the normalised fatigue life is defined as the output future. In all cases, 4 specimens (specimen 1 to specimen 4) were used for training and specimen 5 is kept as an unknown specimen for validation to make a consistent comparison across all modes.

Single-mode learning

In the single-mode model, each model was trained using one modal feature at a time, and each of the six modes was evaluated independently. The input vector X(n) is defined as shown in Equation 18.

$$X(n) = X_i(n) = (f_i(n)/f_i(0))^2 \quad (18)$$

where: $fi(n)$ – natural frequency of mode I at n cycles.

Multi-mode learning

In the multi-mode model, the global structural degradation effects were incorporated, and validation on specimen 5 was performed using a multi-mode vector. The multi-mode feature vector was defined as shown in Equation 19 and Equation 20.

$$X(n) = \begin{bmatrix} X_1(n), X_2(n), X_3(n), \\ X_4(n), X_5(n), X_6(n) \end{bmatrix} \quad (19)$$

$$X(n) = \begin{bmatrix} \left(\frac{f_1(n)}{f_1(0)}\right)^2, \left(\frac{f_2(n)}{f_2(0)}\right)^2, \\ \ldots\ldots\ldots, \left(\frac{f_6(n)}{f_6(0)}\right)^2 \end{bmatrix} \quad (20)$$

Single-mode machine learning model performance

The predictive performance of the single-mode SVR-S model is summarised in Table 9. The predictive performance capability of SVR-S results in strong dependence on modal sensitivity. Mode 1 resulted in poor predictive performance (R^2 = −0.393, RMSE = 0.225, RE = 79.50%), indicating that the fundamental mode is insensitive to the fatigue-induced stiffness degradation, and the low curvature in limited frequency variation reduces its effectiveness as a damage indicator. Greater improvement in prediction performance was noticed with increasing modal order, with mode 4 having the highest performance (R^2 = 0.791, RMSE = 0.087, RE = 20.23%) among all single-mode SVR models. Mode 5 and Mode 6 also resulted in stable prediction capabilities with R^2 = 0.728 and 0.644, respectively. The trend in the results confirms that the higher bending modes provide more sensitive informative features for nonlinear regression mapping between frequency degradation and normalised fatigue life. Overall, SVR-S exhibits reliable predictive performance when damage-sensitive modal features are employed.

The predictive performance of the single-mode GPR-S model is also summarised in Table 9. In the GPR-S model, the prediction accuracy is highly influenced by the selected modal features. Highly unstable predictions were noticed in mode 1 and mode 2 with negative R^2 (−1.095 and −17.164) values and large relative errors (138.97% and 68.14%). These results depict that the lower modes do not offer sufficient

informative features for probabilistic regression mapping under limited training samples. Further, the instability noted in lower modes highlights the sensitivity of GPR-S to noisy features under small training datasets. From mode 3 onwards, the predictive performance improved significantly and mode 4 gave the best performance (R^2 = 0.845, RMSE = 0.075, RE = 17.57%) among all modes, which outperforms the SVR-S model for the same mode. The superior performance of mode 4 in GPR-S was due to the probabilistic framework of the GPR-S model and the ability of GPR-S to model smooth nonlinear degradation behaviour under the input features with strong stiffness reduction correlation. Mode 5 and mode 6 also resulted in reasonably stable predictions with R^2 = 0.692 and 0.64, respectively.

Both single-mode models demonstrated strong modal sensitivity dependence, and mode 4 consistently provided the best predictive performance under both models. GPR-S slightly outperforms SVR-S in mode 4 (R^2 = 0.845 vs 0.791; RE = 17.57% vs 20.23%), whereas SVR-S shows greater stability across moderately sensitive modes (Modes 3–6). The above results confirm that the model performance is primarily governed by feature quality over the algorithm selection. When a quality modal feature is employed, both the single-mode models demonstrated strong predictive performance, whereas both algorithms failed to generalise effectively when weak features were employed. Therefore, modal feature selection plays a critical role in vibration-based fatigue life estimation over the influence of the regression algorithm.

To assess the engineering reliability, the predicted fatigue lives were evaluated using a 2 times error band criterion. For SVR-S as shown in Figure 11, the majority of the predicted fatigue lives corresponding to higher modes lie within the error band and in that the mode 4 resulted in clustering around the equality line, confirming its superior predictive reliability. However, mode 1 resulted in significant deviation with multiple predictions falling outside the error band, which is consistent with the poor R^2 and relative error it has resulted in. In GPR-S, as shown in Figure 12, higher modes (Mode 4 to Mode 6) largely lie within the acceptable band and Mode 4 exhibited much tighter clustering around the prediction line compared to SVR-S. Mode 1 and mode 2 resulted in significant instability, with several predictions falling outside the lower bound of the error band, which confirms the negative R^2 values observed for these modes. The error band analysis further confirms that the predictive performance is primarily governed by modal sensitivity over the algorithm complexity.

Multi-mode machine learning model performance

To investigate the prediction capability when multiple modal features are integrated, a multimode learning model was implemented. In this model, the normalised squared frequency ratios are simultaneously given as input features, and the prediction performance of multimode SVR (SVR-M) as well as multimode GPR (GPR-M) are summarized in Table 10.

SVR-M resulted in an R^2 of 0.783 with RMSE of 0.0889 and a mean relative error of 35.01%. The R^2 value of SVR-M indicates its capability of capturing a significant portion of the nonlinear relationship between modal frequency degradation and normalised fatigue life when multiple modes are considered simultaneously. Noticeably higher relative error suggests that although multi-mode feature integration can stabilise the regression behaviour, the inclusion of less damage-sensitive modes introduces

Table 9. Prediction performance of single-mode machine learning models (SVR-S and GPR-S) for fatigue life estimation using normalised modal frequency features

Mode	SVR single mode			GPR single mode		
	R^2	RMSE	Relative error (%)	R^2	RMSE	Relative error (%)
Mode 1	−0.393	0.225	79.50%	−1.095	0.276	138.97%
Mode 2	0.42	0.145	29.14%	−17.164	0.812	68.14%
Mode 3	0.532	0.13	23.10%	0.451	0.141	33.56%
Mode 4	0.791	0.087	20.23%	0.845	0.075	17.57%
Mode 5	0.728	0.099	23.07%	0.692	0.106	22.98%
Mode 6	0.644	0.114	28.18%	0.64	0.114	31.95%

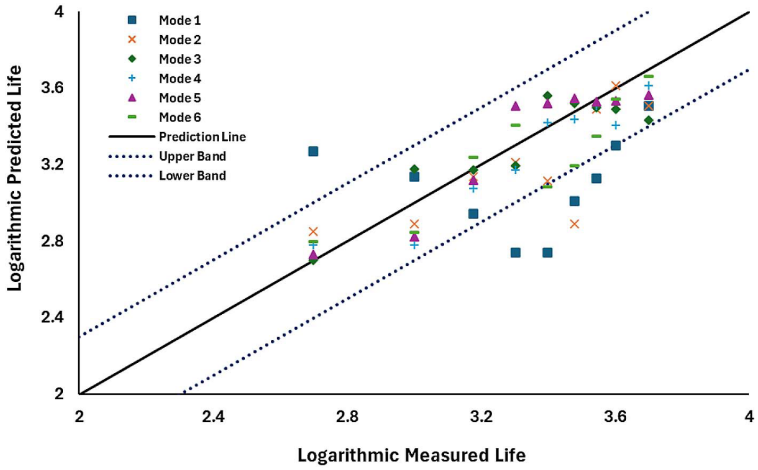

Figure 11. Two-times error band analysis comparing predicted and measured logarithmic fatigue lives obtained using a single-mode Support Vector Regression model

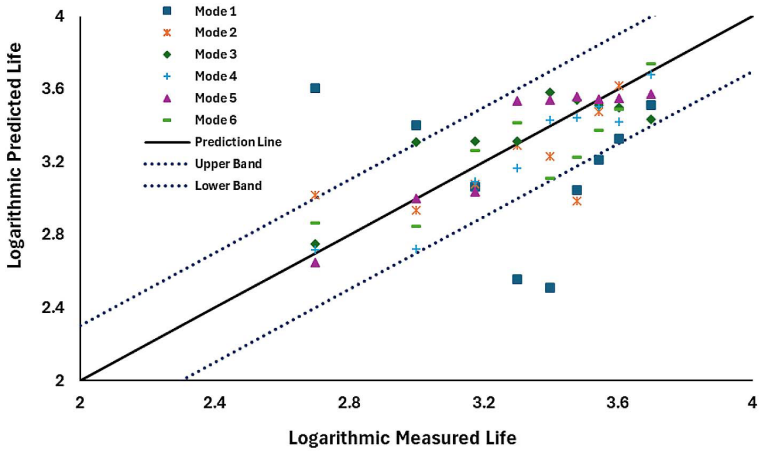

Figure 12. Two-times error band analysis comparing predicted and measured logarithmic fatigue lives obtained using a single-mode Gaussian Process Regression model

additional variability into the prediction process. On the other hand, GPR-M resulted in significant poor performance with $R^2 = -0.0066$, RMSE = 0.1912 and a mean relative error of 54.84%. The near-zero and negative R^2 indicate that the model fails to capture the underlying relationship between the multi-mode frequency features and fatigue life. The limited size of the training dataset relative to the increased dimensionality of the input feature space is the primary reason for resulted degraded performance. With the simultaneous introduction of six modal features, GPR-M becomes highly sensitive to noise and hyperparameter estimation, leading to reduced generalisation capability. The comparison of SVR-M and GPR-M highlights contrasting behaviour under the high-dimensional input features. SVR-M demonstrated relatively better performance due to its structural risk minimisation principle and kernel-based regression capabilities. On the other hand, GPR-M becomes unstable when the dimension of the input features increases without an equivalent increase in the training data.

To assess the reliability of the predictive performance of SVR-M and GPR-M, a 2-times error analysis was performed and depicted in Figure 13. In the SVR-M model, most of the predicted points lie within the acceptable error band with some deviation from the equality line, especially at the lower fatigue life. This shows the ability of the SVR-M model to capture the nonlinear relationship between the multimodal frequency degradation and fatigue life with reasonable stability. In contrast to SVR-M, GPR-M exhibited larger scatter about the equality line, and several predictions fell outside the acceptable error band,

Table 10. Prediction performance of multi-mode machine learning models (SVR-M and GPR-M) for fatigue life estimation using normalised modal frequency features

SVR multi mode			GPR multi mode		
R^2	RMSE	Relative error (%)	R^2	RMSE	Relative error (%)
0.783	0.0889	35.01%	−0.0066	0.1912	54.84%

especially below the lower band. This indicates the tendency of the model to underestimate the fatigue life in most of the cases. This behaviour confirms the lower R^2 and higher relative error of the GPR-M model. Once again, the 2-times error band analysis confirms that the SVR-M provides more consistent and reliable predictions compared to the GPR-M model.

COMPARATIVE PERFORMANCE OF SEMI-EMPIRICAL AND MACHINE LEARNING MODELS

Table 11 shows the comparison of predictive performance of the semi-empirical Mao model and machine learning models SVR-S, GPR-S, SVR-M and GPR-M. These models are assessed using the coefficient of determination, root mean square error and mean relative error. In all single-mode ML models and the semi-empirical Mao model, mode 4 provided the highest predictive performance, indicating its highest sensitivity to the stiffness degradation induced by the fatigue damage. Among the ML models, the GPR-S model using mode 4 achieved the best predictive performance with R^2 = 0.845 and RMSE = 0.075, indicating a strong correlation between the predicted and measured fatigue lives when the most sensitive modal feature is used. SVR-S model using mode 4 also demonstrated good prediction capability (R^2 = 0.791 and RMSE = 0.087) with slightly higher prediction error. However, both single-mode models exhibited strong sensitivity to the modal feature selection. When less informative modes are used as the input feature, the predictive performance significantly deteriorates. With mode 1, SVR-S resulted in a negative R^2 = -0.393 with large prediction error (RE = 79.5%), while the GPR-S with mode 2 showed severe instability with R^2 = −17.164, RMSE = 0.812 and RE = 68.14%. This strongly indicates that single ML models rely heavily on the physical relevance of the selected modal feature.

In the multi-mode framework, SVR-M achieved moderate prediction accuracy, suggesting that combining multiple modal features can stabilise the regression process. In contrast, GPR-M exhibited poor performance, highlighting the GPR sensitivity to dimensional input spaces when the available training dataset is limited. Nevertheless, neither multi-model outperformed the best single-mode model, implying that inclusion of less sensitive modes may introduce additional variability in prediction.

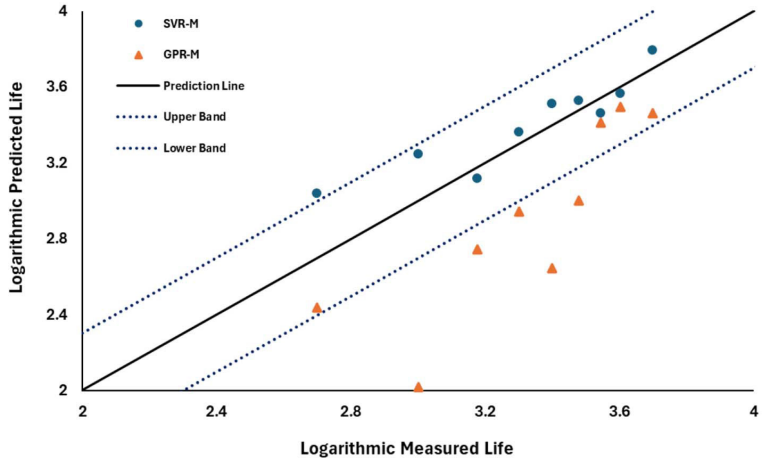

Figure 13. Two-times error band analysis comparing predicted and measured logarithmic fatigue lives obtained using multi-mode ML models (SVR-M and GPR-M)

Table 11. Comparative prediction performance of semi-empirical and machine learning models for fatigue life estimation using modal frequency degradation

Model	Mode		R^2	RMSE	Relative error (%)
SVR-S	Best mode	Mode 4	0.791	0.087	20.23%
	Worst mode	Mode 1	−0.393	0.225	79.50%
GPR-S	Best mode	Mode 4	0.845	0.075	17.57%
	Worst mode	Mode 2	−17.164	0.812	68.14%
SVR-M	Multi-mode		0.783	0.0889	35.01%
GPR-M	Multi-mode		−0.0066	0.1912	54.84%
Mao	Best mode	Mode 4	0.841	0.075	2.88
	Worst mode	Mode 1	-0.159	0.205	29.97

Due to the limited size of the experimental dataset, a leave-one-out cross-validation (LOOCV) strategy was adopted to evaluate the generalisation capability of the machine learning models. In this approach, models were trained using four specimens and validated on the remaining specimen, and the process was repeated iteratively for all five specimens. The reported performance metrics shown in Table 12 correspond to the average values obtained across all validation folds. This approach ensures that each specimen is used for validation while maximising the use of available data for training. It should be noted that the dataset size in the present study is limited due to the experimental effort required for fatigue–modal testing. Machine learning models are generally data-intensive and may exhibit overfitting when trained on small datasets. Therefore, the conclusions regarding machine learning performance in this study are intended to provide comparative insights rather than establish generalizable superiority. Future studies with larger datasets are expected to further improve the reliability and generalisation capability of machine learning models.

Interestingly, the semi-empirical Mao model demonstrated highly competitive performance ($R^2 = 0.841$, RMSE = 0.075, RE = 2.88%), especially when mode 4 is used as the modal indicator. Notably, the best performing ML model, GPR-S using mode-4, produces prediction accuracy that lies between the best and worst performance bounds of the Mao model. While the ML model slightly surpasses the Mao model in terms of R^2, the Mao model exhibits lower relative error. This highlights the effectiveness of physics-based stiffness degradation models for fatigue prognosis.

An interesting observation from the present study is that Mode 4 consistently provides the best prediction performance among all vibration modes, despite higher modes (Modes 5 and 6) having greater theoretical sensitivity to stiffness degradation. This can be explained by considering the trade-off between sensitivity and measurement reliability. While higher modes are more responsive to stiffness changes, they are also associated with lower vibration amplitudes, increased modal density, and potential mode overlap, which can introduce higher experimental noise and uncertainty in frequency extraction. In addition, the single-axis measurement configuration and discrete excitation points may limit the accurate capture of higher-order modal characteristics. As a result, Modes 5 and 6 exhibit increased variability in the experimental data, leading to reduced prediction accuracy. Mode 4, on the other hand, represents an optimal balance between damage sensitivity and measurement stability, resulting in improved model performance.

In addition to prediction accuracy, computational efficiency, as summarised in Table 13, is an important consideration for practical implementation. The semi-empirical models (Mao and Wu) involve direct analytical formulations and require minimal computational effort for both parameter estimation and prediction. In contrast, machine learning models, particularly GPR, involve higher computational cost due to kernel matrix inversion and hyperparameter optimisation, with training complexity scaling cubically with dataset size. SVM models also require hyperparameter tuning, but are relatively efficient for small datasets. Therefore, while machine learning models offer flexibility in capturing nonlinear relationships, semi-empirical models provide significant advantages in terms of computational simplicity and ease of implementation, especially in real-time or resource-constrained applications.

Overall, the modal feature sensitivity plays a more critical role than the algorithm complexity

Table 12. Comparative prediction performance of leave-one-out cross-validation (LOOCV) of machine learning models for fatigue life estimation using modal frequency degradation

Model	Mode	R^2 (Mean±Std)	RMSE (Mean±Std)	Relative error (%)(Mean±Std)
SVR-S	Mode 4	0.78 ± 0.06	0.09±0.01	21.5 ± 4.2
GPR-S	Mode 4	0.83 ± 0.05	0.078 ± 0.008	18.9 ± 3.6
SVR-M	-	0.76 ± 0.07	0.095 ± 0.012	34.1 ± 5.5
GPR-M	-	0.02 ± 0.15	0.19 ± 0.02	55.2 ± 6.8

Table 13. Computational cost comparison

Model	Training cost	Prediction cost	Hyperparameter tuning	Complexity	Remarks
Mao model	Very Low	Very Low	Not required	O(n)	Direct analytical formulation
Wu model	Very Low	Very Low	Not required	O(n)	Direct analytical formulation
SVR	Moderate	Low	Required (C, γ)	$O(n^3)$ for training and O(n) for prediction	Efficient for small datasets
GPR	High	Moderate	Required (kernel params)	$O(n^3)$ for training and $O(n^2)$ for prediction	Computationally intensive

in fatigue life prediction. Although ML models achieved competitive performance when the appropriate modal feature is selected, the semi-empirical model provides comparable or even superior prediction accuracy. These findings suggest that integrating physical degradation mechanisms with data-driven approaches may provide a more reliable framework for vibration-based fatigue life prediction. While both semi-empirical and machine learning approaches are capable of capturing fatigue-induced degradation trends, their performance is governed by the reliability of the input features derived from experimental modal analysis. This highlights that improving feature selection and measurement fidelity can be more impactful than increasing model sophistication in vibration-based fatigue life prediction. The observed performance of the Mao model should therefore be interpreted not solely as an advantage of physics-based modelling, but as a result of its compatibility with stable and physically meaningful modal features. This suggests that future research should prioritise feature engineering and measurement robustness alongside model development for improved fatigue prognosis.

CONCLUSIONS

This study investigated the vibration-based fatigue life prediction of unidirectional GFRP laminates by integrating the experimental fatigue-modal analysis, semi-empirical stiffness degradation models and machine learning approaches. Interrupted modal testing and regression-based prediction models are systematically employed to establish the relationship between natural frequency degradation and interrupted fatigue life. Based on the experiments and predictive analysis, the following conclusions were drawn:

- Fatigue-interrupted modal testing revealed consistent degradation in natural frequencies with respect to increasing fatigue cycles. Higher modes demonstrated greater sensitivity to fatigue damage compared to the fundamental mode.
- The Mao model resulted in more stable prediction behaviour compared to the Wu model due to its power-law degradation formulation. The Mao model effectively captured the early and intermediate life fatigue damage evolution with limited end-of-life data.
- Mao semi empirical model exhibited strong dependence on modal sensitivity. Lower modes showed poor predictive capability, and with higher modes, the prediction accuracy was better. Mode 4 provided the highest predictive accuracy.
- Among the ML frameworks investigated, GPR-S with mode 4 achieved the highest prediction accuracy, outperforming the SVR-S model. Further, the prediction capability of

single-mode ML models is highly sensitive to input future selection when limited training datasets are available.

- SVR-M model exhibited moderate predictive performance, and GPR-M showed unstable performance. The multi-mode approach did not outperform the best single-mode model, indicating that inclusion of less sensitive futures may introduce additional variability in prediction.
- Compared to ML models, the semi-empirical Mao model demonstrated highly competitive performance with limited data availability. This highlights the robustness of physics-based degradation formulations for fatigue prognosis when reliable features are available.
- This study demonstrates that modal sensitivity and feature quality are more critical than algorithm complexity in prediction accuracy. Integrating the physics-based degradation models with data-driven approaches may further improve the robustness and reliability of fatigue prognosis.

Acknowledgement

The authors would like to thank NITTE Meenakshi Institute of Technology, NITTE Deemed to be University, for their continuous support and motivation to carry out this research work.

REFERENCES

1. Harizi W., Chaki S., Bourse G., Ourak M. Damage mechanisms assessment of Glass Fiber-Reinforced Polymer (GFRP) composites using multivariable analysis methods applied to acoustic emission data. Composite Structures. 2022; 289: 115470. https://doi.org/10.1016/j.compstruct.2022.115470
2. Anurag D., Modesar S., Dmytro V., Boutrous K., Mylène DL., Salim C. An overview of damage identification in composite structures—from computational methods to machine learning. Journal of Composite Science. 2025; 9: 683. https://doi.org/10.3390/jcs9120683
3. Xuebing X. and Cheng L. Physics-guided deep learning for damage detection in CFRP composite structures. Composite Structures. 2024; 331: 117889. https://doi.org/10.1016/j.compstruct.2024.117889
4. Aravind P., Gaurav S., Frank B. A straightforward machine learning-based giga-cycle fatigue life regression approach for polymer matrix composites. Results in Engineering. 2025; 28: 108037. https://doi.org/10.1016/j.rineng.2025.108037
5. Vineet K., Raman B., Manoj K. The fatigue of carbon fiber reinforced polymer composites – A review. Materials Today: Proceedings. 2024; 0: 0. https://doi.org/10.1016/j.matpr.2024.06.004
6. Anurag S. and Sunil CJ. Enhancement in fatigue performance of FRP composites with various fillers: A review. Composite Structures. 2023; 309: 116724. https://doi.org/10.1016/j.compstruct.2023.116724
7. Safdar AK., Seyed SRK., Wong KJ., Geralt S., Mohd NT. A fatigue model to predict interlaminar damage of FRP composite laminates subjected to Mode I load. Polymers. 2023; 15: 527. https://doi.org/10.3390/polym15030527
8. Sudhanshu S., Zunjarrao K., Ghanshyam N. Textile-reinforced composite structural-health monitoring systems. Non-Destructive Testing and Evaluation. 2024; 0: 1–28. https://doi.org/10.1080/00405167.2024.2422749
9. Mahendran G., Gopalakrishnan K., Ganesh KM. Vibration-based structural health monitoring of laminated composite beams using finite element modal and harmonic analysis. Journal of Composite Science. 2026; 10: 79. https://doi.org/10.3390/jcs10020079
10. Talreja R. Fatigue of composite materials: Damage mechanisms and fatigue-life diagrams. Proceedings of the Royal Society of London. Series A, Mathematical and Physical Sciences. 1981; 378: 461–475. https://www.jstor.org/stable/2397144
11. Jianxiong G., Pengnian Z., Yiping Y., Zhifeng W., Rongxia X. Strength and stiffness degradation modeling and fatigue life prediction of composite materials based on a unified fatigue damage model. Engineering Failure Analysis. 2022; 137: 106290. https://doi.org/10.1016/j.engfailanal.2022.106290
12. Sreekanth TG., Senthilkumar M., Manikanta RS. Vibration-based delamination evaluation in GFRP composite beams using ANN. Polymers and Polymer Composites. 2021; 29: 317–324. https://doi.org/10.1177/09673911211003399
13. Zhihong L., Karthik RR., Ching-Tai NG., Zhifang Z., Jiyang F. Vibration-based prediction of residual fatigue life for composite laminates through frequency measurements. Composite Structures. 2024; 329: 117771. https://doi.org/10.1016/j.compstruct.2023.117771
14. Abdeldjebar Z., Idir B., Samir K., Abdelmoumin OB., Djilali B., Magd AW. Damage detection in GFRP composite structures by improved artificial neural network using new optimization techniques. Composite Structures. 2023; 305: 116475. https://doi.org/10.1016/j.compstruct.2022.116475
15. Yang Y., Yao Z., Xiaokun T. Review on vibration-based structural health monitoring techniques and technical codes. Symmetry. 2021; 13: 1998. https://doi.org/10.3390/sym13111998

16. Zheng-Qiang C., Wei T., Jun-Jiang X. Progressive damage modelling and fatigue life prediction of Plain-weave composite laminates with Low-velocity impact damage. Composite Structures. 2021; 273: 114262. https://doi.org/10.1016/j.compstruct.2021.114262
17. Mao H. and Mahadevan S. Fatigue damage modelling of composite materials. Composite Structures. 2002; 58: 405–410. https://doi.org/10.1016/S0263-8223(02)00126-5
18. Wu F. and Yao W. A fatigue damage model of composite materials. International Journal of Fatigue. 2010; 32: 134–138. https://doi.org/10.1016/j.ijfatigue.2009.02.027
19. Yang JN., Jones DL., Yang SH., Meskini A. A stiffness degradation model for graphite/epoxy laminates. Journal of Composite Materials. 1990: 24: 753–769. https://doi.org/10.1177/002199839002400705
20. Zong J. and Yao W. Fatigue life prediction of composite structures based on online stiffness monitoring. Journal of Reinforced Plastics and Composites. 2017; 36: 1038–1057. https://doi.org/10.1177/0731684417701198
21. Aravind P., Gaurav S., Frank B. A straightforward machine learning-based giga-cycle fatigue life regression approach for polymer matrix composites. Results in Engineering. 2025; 28: 108037. https://doi.org/10.1016/j.rineng.2025.108037
22. Aleksander K., Dariusz S., Łukasz P. Gaussian process for machine learning-based fatigue life prediction model under multiaxial stress–strain conditions. Materials. 2022; 15: 7797. https://doi.org/10.3390/ma15217797
23. Haijie W., Bo L., Jianguo G., Fu-Zhen X. Machine learning-based fatigue life prediction of metal materials: Perspectives of physics-informed and data-driven hybrid methods. Engineering Fracture Mechanics. 2023; 284: 109242. https://doi.org/10.1016/j.engfracmech.2023.109242
24. Ajeesh Suresh N. and Rajamohan G. Surrogate model-assisted reliability-based design of tapered composite tubes considering global buckling failure. Mechanics Based Design of Structures and Machines. 2025; 0: 1–36. https://doi.org/10.1080/15397734.2025.2549469
25. Jingjing G., Cunjun W., Zili X., Jun W., Song Y., Zhen W. Gaussian process regression based remaining fatigue life prediction for metallic materials under two-step loading. International Journal of Fatigue. 2022; 158: 106730. https://doi.org/10.1016/j.ijfatigue.2022.106730
26. Wojciech M., Dariusz R., Sebastian F., Ricardo B., Shun-Peng Z., Reza MN. Fractographic-fractal dimension correlation with crack initiation and fatigue life for notched aluminium alloys under bending load. Engineering Failure Analysis. 2023; 149: 107285. https://doi.org/10.1016/j.engfailanal.2023.107285
27. Yuequan B. and Hui L. Machine learning paradigm for structural health monitoring. Structural Health Monitoring. 2020; 20: 1353–1372. https://doi.org/10.1177/1475921720972416